

Investigation of Nonequilibrium Internal Energy Excitation in Shock Waves by means of a Spectral-Lagrangian Boltzmann Solver

Alessandro Munafò*, Jeffrey R. Haack[†], Irene M. Gamba** and Thierry E. Magin*

*Aeronautics/Aerospace department, von Karman Institute for Fluid Dynamics, Chaussée de Waterloo 72, 1640 Rhode-Saint-Genèse, Belgium

[†]Department of Mathematics, The University of Texas at Austin, 201 E. 24th Street, Austin, TX 78712, USA

**Department of Mathematics & Institute for Computational and Engineering Sciences, The University of Texas at Austin, 201 E. 24th Street, Austin, TX 78712, USA

Abstract. We propose to extend an existing spectral-Lagrangian numerical method for the Boltzmann equation for a pure gas (without internal energy) to a multi energy level gas. The numerical method is based on the weak form of the collision operator and can be used with any type of cross-section model. The formulation is developed in order to account for both elastic and inelastic collisions, the latter being responsible for internal energy excitation. Applications focus on the investigation of nonequilibrium flows across normal shock waves. Numerical solutions are obtained for both pure gases and mixtures at different values of the free-stream Mach number. Computational results are compared with those obtained by means of the DSMC method in order to assess the accuracy of the proposed numerical method.

Keywords: Boltzmann Equation, Shock Waves, Nonequilibrium Flows, Internal Energy, Spectral Methods

PACS: 02.60.Cb, 47.45.Ab, 47.70.Nd, 82.20.Rp

INTRODUCTION

Possible applications of rarefied gas dynamics include the computation of the flowfield around spacecrafts entering planetary atmospheres and the flow in hypersonic wind tunnels. Understanding rarefied gas effects in aerospace applications is important for an accurate calculation of the aerodynamic coefficients during the early phase of the entry of a space capsule into a planetary atmosphere, prediction of the heat flux experienced by ballutes during entry and descent, and also a correct interpretation of experimental measurements.

Attempts to compute rarefied flows by means of a hydrodynamic description based on the Navier-Stokes equations give inaccurate results due to the failure of Newton's law for the stress tensor and Fourier's law for the heat flux vector in the rarefied regime [1]. The Boltzmann equation provides a statistical description of dilute gaseous systems valid from the rarefied to the hydrodynamic regime [1]. It describes the evolution of the species distribution function in the phase-space. Once the distribution function of each species is known, it is possible to compute macroscopic observables such as density, hydrodynamic velocity and temperature by means of suitable moments. The computation of numerical solutions of the Boltzmann equation is not trivial. This is due to the integro-differential nature of the equation. A further source of difficulty is the high dimensionality of the problem (numerical solutions must be sought in the phase-space). Stochastic-like solutions of the Boltzmann equation can be obtained by means of the Direct-Simulation-Monte-Carlo (DSMC) method [2, 3]. The former is a particle-based technique and has proven to be accurate [3]. However, it shares the drawbacks of stochastic methods, the main one being the presence of noise in the numerical results [2]. The former problem affects, in particular, the accuracy of the solution for low speed and unsteady flows. Parallel to the development of the DSMC method, deterministic numerical methods for the Boltzmann equation have been proposed. These comprise, among all, discrete velocity models [4, 5] and spectral methods [6, 7]. The main advantage of a deterministic method over the DSMC technique is that the numerical solution obtained is not affected by numerical noise. Deterministic methods can also be applied to flow problems in the hydrodynamic and transition regime, for which the use of the DSMC method becomes prohibitively expensive [8].

In the present work, we propose to extend an existing spectral-Lagrangian numerical method [6] for the Boltzmann equation for a pure gas (without internal energy) to a multi energy level gas. The numerical method is based on the weak form of the collision operator and can be used with any type of cross-section model. The formulation is developed

in order to account for both elastic and inelastic collisions, the latter being responsible for internal energy excitation. The paper is structured as follows. The physical model considered is introduced. After that, the proposed numerical method is explained. Next, preliminary results obtained for the flow across a normal shock wave of mixture of gases without internal energy are discussed and analyzed. Conclusions and future work are outlined in the last section.

PHYSICAL MODELING

Simplifying Assumptions and Conventions

The physical model used in the present work is based on the following assumptions and conventions [9]:

1. The gas mixture is composed of identical particles.
2. Particles have discrete internal energy levels:
 - The indices of energy levels are stored in the set $I_S = \{1, \dots, N_S\}$, N_S being the number of species.
 - The mass of the species (energy level) $i \in I_S$ is m_i .
 - The degeneracy and the energy of the energy level $i \in I_S$ are g_i and E_i , respectively.
3. Only binary collisions are accounted for:

$$i + j = i' + j', \quad i, j, i', j' \in I_S. \quad (1)$$

- Elastic collision: $i = i'$ and $j = j'$.
- Inelastic collision: $(i', j, j') \in C_i^{\text{in}}$. The set C_i^{in} stores the ordered triplets (i', j, j') for all the possible inelastic collisions involving the species i as reactant in Eq. (1) and is defined as:

$$C_i^{\text{in}} = \left\{ (i', j, j') \in \left[I_S \times I_S \times I_S \setminus \bigcup_{s \in I_S} (i, s, s) \right] \right\}, \quad i \in I_S. \quad (2)$$

4. The presence of chemical reactions (such as dissociation and ionization) and external force fields is neglected.

Governing Equations

Based on the hypothesis introduced in the previous section, a Boltzmann equation can be written for the velocity distribution function $f_i(\mathbf{x}, \mathbf{v}, t)$ of the species $i \in I_S$:

$$\frac{\partial f_i}{\partial t} + \mathbf{v} \cdot \frac{\partial f_i}{\partial \mathbf{x}} = \sum_{j \in I_S} Q_{ij}(\mathbf{v}) + \sum_{(i', j, j') \in C_i^{\text{in}}} Q_{ij}^{i'j'}(\mathbf{v}), \quad i \in I_S. \quad (3)$$

In Eq. (3) the quantities $Q_{ij}(\mathbf{v})$ and $Q_{ij}^{i'j'}(\mathbf{v})$ are, respectively, the elastic and inelastic collision operators [1]:

$$Q_{ij}(\mathbf{v}) = \iint_{\substack{\mathbf{w} \in \mathcal{R}^3, \\ \omega' \in S^2}} [f_i(\mathbf{v}') f_j(\mathbf{w}') - f_i(\mathbf{v}) f_j(\mathbf{w})] \sigma_{ij} u d\omega' d\mathbf{w}, \quad i, j \in I_S, \quad (4)$$

$$Q_{ij}^{i'j'}(\mathbf{v}) = \iint_{\substack{\mathbf{w} \in \mathcal{R}^3, \\ \omega' \in S^2}} \left[\frac{g_i g_j}{g_{i'} g_{j'}} f_{i'}(\mathbf{v}') f_{j'}(\mathbf{w}') - f_i(\mathbf{v}) f_j(\mathbf{w}) \right] \sigma_{ij}^{i'j'} u d\omega' d\mathbf{w}, \quad i \in I_S, (i', j, j') \in C_i^{\text{in}}. \quad (5)$$

In Eqs. (4) - (5), \mathbf{v} and \mathbf{w} are, respectively, the velocities of the species i and j , u is the relative velocity magnitude $u = |\mathbf{v} - \mathbf{w}|$, ω' is the solid angle of the scattering direction, and σ_{ij} and $\sigma_{ij}^{i'j'}$ are, respectively, the differential cross-sections for the elastic and inelastic collision associated to the binary interaction given in Eq. (1). It is important to mention that the potential model used to obtain the differential cross-section is general and not restricted to hard-sphere

interactions. As usual, primed variables in Eqs. (4) - (5) (and in what follows) refer to post-collisional values. Their values are related to pre-collisional values through the conservation of momentum and energy:

$$m_i \mathbf{v} + m_j \mathbf{w} = m_{i'} \mathbf{v}' + m_{j'} \mathbf{w}', \quad (6)$$

$$\frac{1}{2} m_i v^2 + E_i + \frac{1}{2} m_j w^2 + E_j = \frac{1}{2} m_{i'} v'^2 + E_{i'} + \frac{1}{2} m_{j'} w'^2 + E_{j'}, \quad i, j, i', j' \in I_S. \quad (7)$$

Note that for a pure gas with internal energy the mass of all the particles are identical ($m_i = m_j = m_{i'} = m_{j'}$).

Eq. (3) may also be used for the case of a mixture of monatomic gases without internal energy. In this situation, $m_i = m_{i'}$ and $m_j = m_{j'}$. Moreover only elastic collisions occur and all the terms $Q_{ij}^{i'j'}(\mathbf{v})$ in Eq. (3) are zero.

The Fourier Transform of the Elastic and Inelastic Collision Operators

The numerical method in use in the present work makes use of the Fourier transform of the elastic and inelastic collision operators [10] (Eqs. (4) - (5), respectively). The former can be computed based on their weak form:

$$\int_{\mathbf{v} \in \mathfrak{R}^3} \Phi_i(\mathbf{v}) Q_{ij}(\mathbf{v}) d\mathbf{v} = \iiint_{\substack{\mathbf{w} \in \mathfrak{R}^3, \mathbf{v} \in \mathfrak{R}^3, \\ \omega' \in S^2}} f_i(\mathbf{v}) f_j(\mathbf{w}) [\Phi_i(\mathbf{v}') - \Phi_i(\mathbf{v})] \sigma_{ij} u d\omega' d\mathbf{w} d\mathbf{v}, \quad i, j \in I_S, \quad (8)$$

$$\int_{\mathbf{v} \in \mathfrak{R}^3} \Phi_i(\mathbf{v}) Q_{ij}^{i'j'}(\mathbf{v}) d\mathbf{v} = \iiint_{\substack{\mathbf{w} \in \mathfrak{R}^3, \mathbf{v} \in \mathfrak{R}^3, \\ \omega' \in S^2}} f_i(\mathbf{v}) f_j(\mathbf{w}) [\Phi_{i'}(\mathbf{v}') - \Phi_i(\mathbf{v})] \sigma_{ij}^{i'j'} u d\omega' d\mathbf{w} d\mathbf{v}, \quad i \in I_S, (i', j, j') \in C_i^{\text{in}}, \quad (9)$$

where the function $\Phi_i(\mathbf{v})$ in Eqs. (8) - (9) is a smooth test function of the velocity \mathbf{v} . The substitution of a Fourier velocity mode $\Phi_i(\mathbf{v}) = (2\pi)^{-3/2} \exp(-i\boldsymbol{\zeta} \cdot \mathbf{v})$ in Eqs. (8) - (9) gives the Fourier transform of the elastic and inelastic collision operators and, after some algebraic manipulation (similar to [6]), the following expressions are obtained:

$$\hat{Q}_{ij}(\boldsymbol{\zeta}) = \frac{1}{(\sqrt{2\pi})^3} \int_{\boldsymbol{\xi} \in \mathfrak{R}^3} \hat{f}_i(\boldsymbol{\zeta} - \boldsymbol{\xi}) \hat{f}_j(\boldsymbol{\xi}) \tilde{G}_{ij}(\boldsymbol{\zeta}, \boldsymbol{\xi}) d\boldsymbol{\xi}, \quad i, j \in I_S, \quad (10)$$

$$\hat{Q}_{ij}^{i'j'}(\boldsymbol{\zeta}) = \frac{1}{(\sqrt{2\pi})^3} \int_{\boldsymbol{\xi} \in \mathfrak{R}^3} \hat{f}_i(\boldsymbol{\zeta} - \boldsymbol{\xi}) \hat{f}_j(\boldsymbol{\xi}) \tilde{G}_{ij}^{i'j'}(\boldsymbol{\zeta}, \boldsymbol{\xi}) d\boldsymbol{\xi}, \quad i \in I_S, (i', j, j') \in C_i^{\text{in}}. \quad (11)$$

In Eqs. (10) - (11), the quantities \hat{f}_i and \hat{f}_j are, respectively, the Fourier transform of the distribution functions of the species i and j , while the quantities $\tilde{G}_{ij}(\boldsymbol{\zeta}, \boldsymbol{\xi})$ and $\tilde{G}_{ij}^{i'j'}(\boldsymbol{\zeta}, \boldsymbol{\xi})$ are weight functions defined as:

$$\tilde{G}_{ij}(\boldsymbol{\zeta}, \boldsymbol{\xi}) = \iint_{\substack{\mathbf{u} \in \mathfrak{R}^3, \\ \omega' \in S^2}} u \sigma_{ij} \left\{ \exp \left[-i \frac{\mu_{ij}}{m_i} \boldsymbol{\zeta} \cdot (\mathbf{u}' - \mathbf{u}) \right] - 1 \right\} \exp(-i\boldsymbol{\xi} \cdot \mathbf{u}) d\omega' d\mathbf{u}, \quad i, j \in I_S, \quad (12)$$

$$\tilde{G}_{ij}^{i'j'}(\boldsymbol{\zeta}, \boldsymbol{\xi}) = \iint_{\substack{\mathbf{u} \in \mathfrak{R}^3, \\ \omega' \in S^2}} u \sigma_{ij}^{i'j'} \left\{ \exp \left[-i \frac{\mu_{ij}}{m_i} \boldsymbol{\zeta} \cdot (\mathbf{u}' - \mathbf{u}) \right] - 1 \right\} \exp(-i\boldsymbol{\xi} \cdot \mathbf{u}) d\omega' d\mathbf{u}, \quad i \in I_S, (i', j, j') \in C_i^{\text{in}}. \quad (13)$$

In Eqs. (12) - (13) the quantity $\mu_{ij} = m_i m_j / (m_i + m_j)$ is the reduced mass of the species i and j . From Eqs. (10) - (11), the following observations can be made:

1. The Fourier transform of the elastic and inelastic collision operators can be written as weighted convolutions in the Fourier space, the weights being the functions $\tilde{G}_{ij}(\boldsymbol{\zeta}, \boldsymbol{\xi})$ and $\tilde{G}_{ij}^{i'j'}(\boldsymbol{\zeta}, \boldsymbol{\xi})$, respectively [6].
2. The weight functions $\tilde{G}_{ij}(\boldsymbol{\zeta}, \boldsymbol{\xi})$ and $\tilde{G}_{ij}^{i'j'}(\boldsymbol{\zeta}, \boldsymbol{\xi})$ depend only on the cross-section model in use. No dependence on the value of the species distribution function occurs. This fact can be exploited by a computational method (see next section) that makes use of Eqs. (10) - (11) for the numerical evaluation of the elastic and inelastic collision operators (the weight associated to each interaction can be pre-computed [11]).
3. Since in the definition provided by Eqs. (12) - (13) no assumption is done on the differential cross-section model, anisotropic interactions can also be taken into account [12].

NUMERICAL METHOD

Numerical solutions to Eq. (3) are sought for 1D flows. Operator splitting is used [6] (due to its ease of implementation and low memory requirements when compared with unsplit implicit methods in the phase-space). Given the numerical solution at the time-level t^n , the solution at the next time-level t^{n+1} is computed as follows:

$$f_i(t^{n+1}) = \mathcal{C}_{\Delta t}(\mathcal{A}_{\Delta t}(f_i(t^n))), \quad i \in \mathbf{I}_S. \quad (14)$$

The operators $\mathcal{A}_{\Delta t}$ and $\mathcal{C}_{\Delta t}$ in Eq. (14) are those of the following differential problems related to Eq. (3):

1. Collisionless Boltzmann equation (transport step - operator $\mathcal{A}_{\Delta t}$):

$$\frac{\partial f_i}{\partial t} + v_x \frac{\partial f_i}{\partial x} = 0, \quad i \in \mathbf{I}_S. \quad (15)$$

2. Space homogeneous Boltzmann equation (collision step - operator $\mathcal{C}_{\Delta t}$):

$$\frac{\partial f_i}{\partial t} = \sum_{j \in \mathbf{I}_S} \mathcal{Q}_{ij}(\mathbf{v}) + \sum_{(i', j') \in \mathbf{C}_i^{\text{in}}} \mathcal{Q}_{i'j'}(\mathbf{v}), \quad i \in \mathbf{I}_S. \quad (16)$$

The combination of the operators provided by Eq. (14) results in a first order time accurate scheme. This is perfectly acceptable if only steady solutions are of interest (as it is the case for the present work). The accuracy in space is influenced by the method used for the advection step (Eq. (15)).

The advection step is performed by means of a cell centered finite volume method [13]. A uniform grid on the x -axis is assumed and Eq. (15) is then discretized on the former (for each velocity node of the velocity domain - see below) by using a second order slope-limited upwind scheme [14] (with van Albada's slope limiter [13]). The integration in time is performed by means of the forward Euler method.

For the collision step, Eq. (16) is integrated in time by means of the forward Euler method. The application of the former requires the evaluation at the time-level t^n of all the collision operators on the right-hand-side of Eq. (16). This is possible only by applying:

1. A discretization of the velocity space,
2. An algorithm for the evaluation of each collision operator,

presented in more details in the following next two subsections.

Velocity Space Discretization

The discrete velocity nodes are chosen within a cube in the space $(O; v_x, v_y, v_z)$ centered at the origin and with side semi-length L_v . A uniform grid of N_v nodes along the v_x , v_y and v_z directions is assumed and, after introducing the set $\mathbf{I}_v = \{0, \dots, N_v - 1\}$ for sake of clarity, the individual velocity nodes are computed as:

$$v_{k_i} = -L_v + k_i \Delta v, \quad k_i \in \mathbf{I}_v, \quad i = x, y, z, \quad (17)$$

where the velocity spacing Δv in Eq. (17) is $\Delta v = 2L_v/N_v$. A velocity grid in the Fourier velocity space $(O; \zeta_x, \zeta_y, \zeta_z)$ is also defined:

$$\zeta_{\varepsilon_i} = -L_\eta + \varepsilon_i \Delta \eta, \quad \varepsilon_i \in \mathbf{I}_v, \quad i = x, y, z. \quad (18)$$

The velocity spacing $\Delta \eta$ and the semi-length L_η of the discretized Fourier velocity domain are assumed to satisfy the relations:

$$\Delta v \Delta \eta = 2\pi/N_v, \quad L_\eta = 2L_v/N_v, \quad (19)$$

in order to use the Fast-Fourier-Transform (FFT) algorithm [6] in the evaluation of the Fourier and inverse Fourier transforms (see below).

Algorithm for the Evaluation of the Collision Operator

The following algorithm is used for the evaluation of the collision operator associated to the interaction between species i and j (whether elastic or inelastic) given by Eq. (1):

1. Compute the Fourier transforms $\hat{f}_{i,j}(\zeta) = \mathcal{F}(f_{i,j}(\mathbf{v})) \rightarrow O(N_v^3 \log N_v)$.
2. For N_v^3 Fourier velocity nodes compute the Fourier transform of the collision operator $Q_{ij}(\mathbf{v})$ by means of:

$$\hat{Q}_{ij}(\zeta) = \int \hat{f}_i(\zeta - \xi) \hat{f}_j(\xi) \tilde{G}_{ij}(\zeta, \xi) d\xi \rightarrow O(N_v^3).$$

3. Compute the inverse Fourier transform $\tilde{Q}_{ij}(\mathbf{v}) = \mathcal{F}^{-1}(\hat{Q}_{ij}(\zeta)) \rightarrow O(N_v^3 \log N_v)$.
4. For N_v^3 velocity nodes enforce conservation through the solution of a constrained optimization problem:

$$Q_{ij}(\mathbf{v}) = \text{Opt}(\tilde{Q}_{ij}(\mathbf{v})) \rightarrow O(N_v^3).$$

The global cost of the algorithm is $O(N_v^6)$ (per interaction) and the last step is performed in order to ensure conservation of mass, momentum and energy during collisions. This approach was originally proposed and formulated in [6] for the case of a simple gas without internal energy. In the present work, an extension of the original method to mixtures with internal energy is proposed. Elastic and inelastic collisions are treated separately and the enforcement of conservation of macroscopic moments is imposed through the following constrained optimization problems:

1. Elastic collisions:

$$\mathcal{P}_{\text{el}} = \left\{ \min \sum_{i,j \in \text{I}_S} \|\tilde{\mathbf{Q}}_{ij} - \mathbf{Q}_{ij}\|_2^2, \sum_{i,j \in \text{I}_S} \mathbf{C}_{\text{eli}} \mathbf{Q}_{ij} = \mathbf{0}_{N_s+4} \right\}. \quad (20)$$

2. Inelastic collisions:

$$\mathcal{P}_{\text{in}} = \left\{ \min \sum_{i \in \text{I}_S} \sum_{(i',j,j') \in \text{C}_i^{\text{in}}} \|\tilde{\mathbf{Q}}_{ij}^{i',j,j'} - \mathbf{Q}_{ij}^{i',j,j'}\|_2^2, \sum_{i \in \text{I}_S} \sum_{(i',j,j') \in \text{C}_i^{\text{in}}} \mathbf{C}_{\text{ini}} \mathbf{Q}_{ij}^{i',j,j'} = \mathbf{0}_5 \right\}. \quad (21)$$

In Eqs. (20) - (21), the vectors \mathbf{Q}_{ij} and $\mathbf{Q}_{ij}^{i',j,j'}$ store the values of the operators $Q_{ij}(\mathbf{v})$ and $Q_{ij}^{i',j,j'}(\mathbf{v})$, respectively, on the discrete velocity nodes given by Eq. (17), while the matrices \mathbf{C}_{eli} and \mathbf{C}_{ini} are integration matrices whose k -th columns are:

$$(\mathbf{C}_{\text{eli}})_k = \Omega_k \left[m_i \delta_{il} \quad m_i v_{k_x} \quad m_i v_{k_y} \quad m_i v_{k_z} \quad \frac{1}{2} m_i V_k^2 \right]^T, \quad i, l \in \text{I}_S, \quad (22)$$

$$(\mathbf{C}_{\text{ini}})_k = \Omega_k \left[m_i \quad m_i v_{k_x} \quad m_i v_{k_y} \quad m_i v_{k_z} \quad \frac{1}{2} m_i V_k^2 + E_i \right]^T, \quad i \in \text{I}_S, \quad (23)$$

where $V_k^2 = v_{k_x}^2 + v_{k_y}^2 + v_{k_z}^2$ and Ω_k is the integration weight associated to the velocity node $k = (k_x, k_y, k_z)$. The structure of the matrices in Eqs. (22) - (23) reflects the fact that there exists a set of $N_s + 4$ collisional invariants for elastic collisions (the single species mass, the global momentum and energy), while, for inelastic collisions, the number of collisional invariants is equal to 5 (the global mass, momentum and energy) [1, 15].

It can be shown that the solutions to the above constrained optimization problems (Eqs. (20) - (21)) are:

1. Elastic collisions:

$$\mathbf{Q}_{ij} = \tilde{\mathbf{Q}}_{ij} - \frac{1}{N_s} \mathbf{C}_{\text{eli}}^T \left(\sum_{p \in \text{I}_S} \mathbf{C}_{\text{elp}} \mathbf{C}_{\text{elp}}^T \right)^{-1} \left(\sum_{p,q \in \text{I}_S} \mathbf{C}_{\text{elp}} \tilde{\mathbf{Q}}_{pq} \right), \quad i, j \in \text{I}_S. \quad (24)$$

2. Inelastic collisions:

$$\mathbf{Q}_{ij}^{i',j,j'} = \tilde{\mathbf{Q}}_{ij}^{i',j,j'} - \frac{1}{N_{\text{in}}} \mathbf{C}_{\text{ini}}^T \left(\sum_{p \in \text{I}_S} \mathbf{C}_{\text{in}p} \mathbf{C}_{\text{in}p}^T \right)^{-1} \left(\sum_{p \in \text{I}_S} \sum_{(p',q,q') \in \text{C}_p^{\text{in}}} \mathbf{C}_{\text{in}p} \tilde{\mathbf{Q}}_{pq}^{p',q'} \right), \quad i \in \text{I}_S, (i',j,j') \in \text{C}_i^{\text{in}}, \quad (25)$$

with $N_{\text{in}} = N_s(N_s^2 - 1)$.

COMPUTATIONAL RESULTS

The numerical method of the previous section has been implemented in a parallel C code. Parallelization is performed by means of the OpenMP library [16]. The GSL [17] and FFTW3 [18] libraries are used, respectively, for vector/matrix manipulation and the implementation of the FFT and inverse FFT algorithms.

All computational results are compared with those obtained by means of the DSMC code presented in [19].

Flow across a Normal Shock Wave in Ar

In order to assess the accuracy of the original numerical method [6], it was decided to compute the flow across a normal shock wave in Ar. The free-stream values for pressure and temperature are 6.25 Pa and 300 K, respectively. Three different values of the free-stream Mach number are considered. The numerical values for the former are given in Table 1 together with those for the N_V and L_V parameters. In all the cases the hard-sphere (HS) collision model [1, 2] is used. The numerical values for the Ar mass and diameter are taken from [2].

TABLE 1. Simulation parameters.

	M_∞	N_V	L_V [m/s]
1	1.5	24	2250
2	3.38	32	3700
3	6.5	44	6500

Figure 1 shows the kinetic temperature (T) and the parallel and transverse temperatures (T_x and T_y , respectively). In all the cases presented here, the parallel temperature T_x experiences an overshoot, reaches a local maximum and then relax towards the value corresponding to the post-shock conditions. This flowfield feature (observed for the first time in DSMC simulations [2]) is more and more enhanced when increasing the free-stream Mach number and is directly related to the distortion (along the x -axis) the velocity distribution function experiences while the flow crosses the shock wave. The kinetic and transverse temperatures, on the contrary, show a monotone increase from the pre-shock till the post-shock value. For both cases shown in Fig. 1 the agreement with the DSMC results is excellent. The same conclusion can be drawn from Fig. 2 showing a comparison for the x component of the heat flux vector and the xx component of the stress tensor.

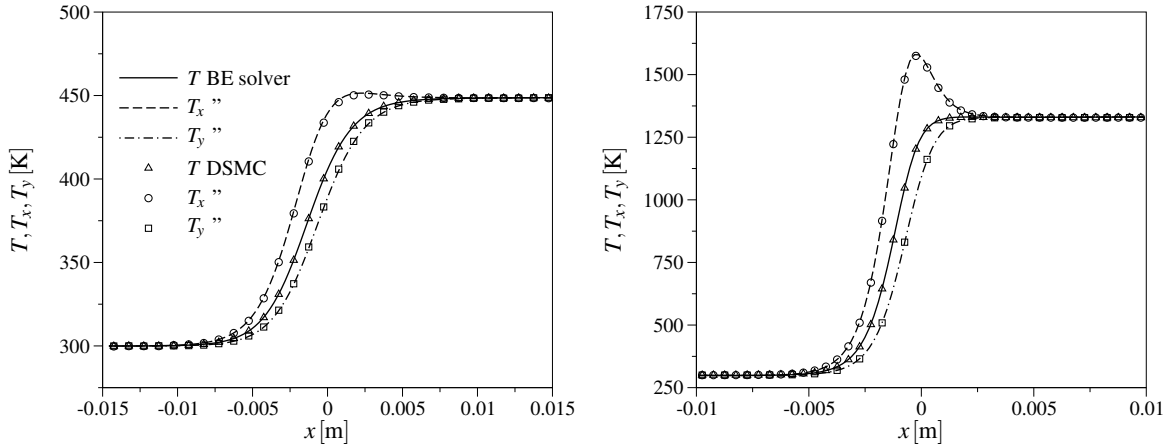


FIGURE 1. Kinetic, parallel and transverse temperatures for the $M_\infty = 1.5$ case (left) and the $M_\infty = 3.38$ case (right) (lines BE solver - symbols DSMC).

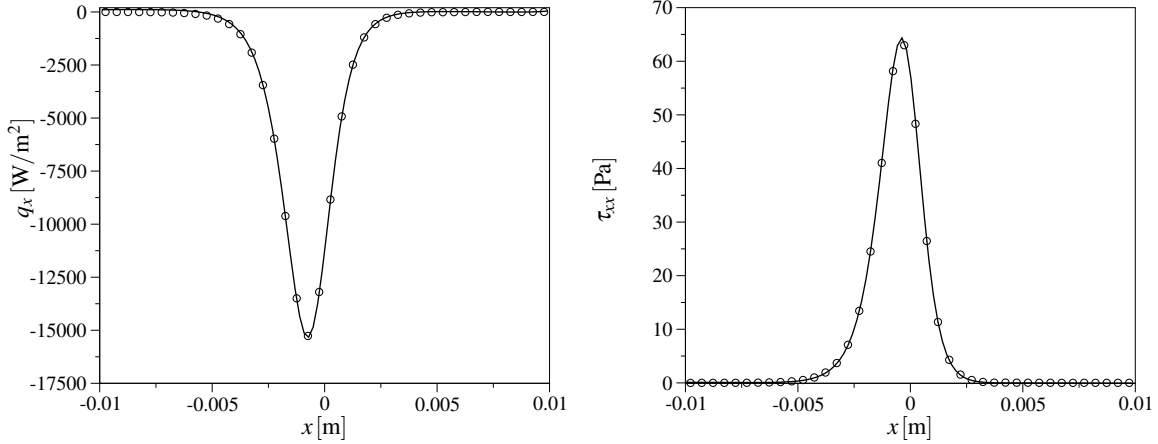


FIGURE 2. Heat flux for the $M_\infty = 3.38$ case (left) and stress tensor for the $M_\infty = 6.5$ case (right) (lines BE solver - symbols DSMC).

Flow across a Normal Shock Wave in a Ne - Ar Mixture

After assessing the accuracy of the original numerical method [6], its extension to mixtures (presented before) was tested on the computation of the flow across a normal shock wave in a binary inert gas mixture made of Ne and Ar. A peculiar aspect of this testcase is the species separation occurring within the shock wave. The former is due to the mass difference between the two species [2] with the lighter species experiencing the compression sooner than the heavier one. The free-stream values of pressure, temperature and Mach number are 8.3 Pa, 300 K and 2, respectively. The mass fractions of Ne and Ar are set to 0.34 and 0.66, respectively, while for the simulation parameters N_v and L_v the values 22 and 2500 m/s, respectively, are used. The HS collision model is used and the numerical values for the species mass and diameter are taken from [2].

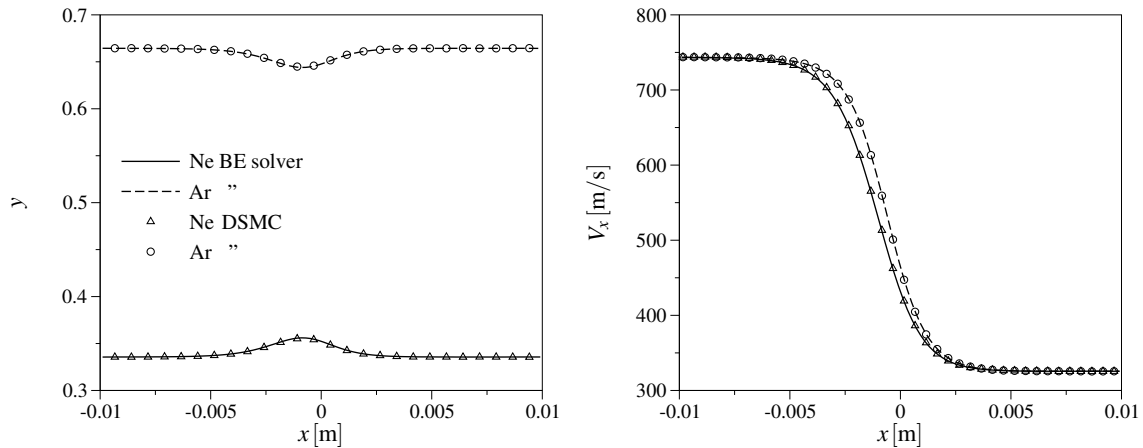


FIGURE 3. Mass fractions (left) and velocity (right) of Ne and Ar (lines BE solver - symbols DSMC).

Figure 3 shows the species mass fractions and velocities across the shock wave. The Ne (whose mass is lower than that of Ar) experiences the compression within the shock sooner than the Ar does (as it can be seen from the velocity variation). This induces an accumulation of Ne atoms in the front part of the shock wave leading, in turn, to a local chemical composition variation. This effect progressively disappears while the flow approaches the post-shock equilibrium state (where no species separation exists) and the chemical composition assumes the same value as that of the free-stream. The species separation can also be appreciated from Fig. 4 showing the species kinetic and parallel temperatures. For each species, the parallel temperature shows the same behavior as that of the simple gas case with the local maximum being more pronounced for the heavier species (Ar). The comparison with the DSMC results is again excellent.

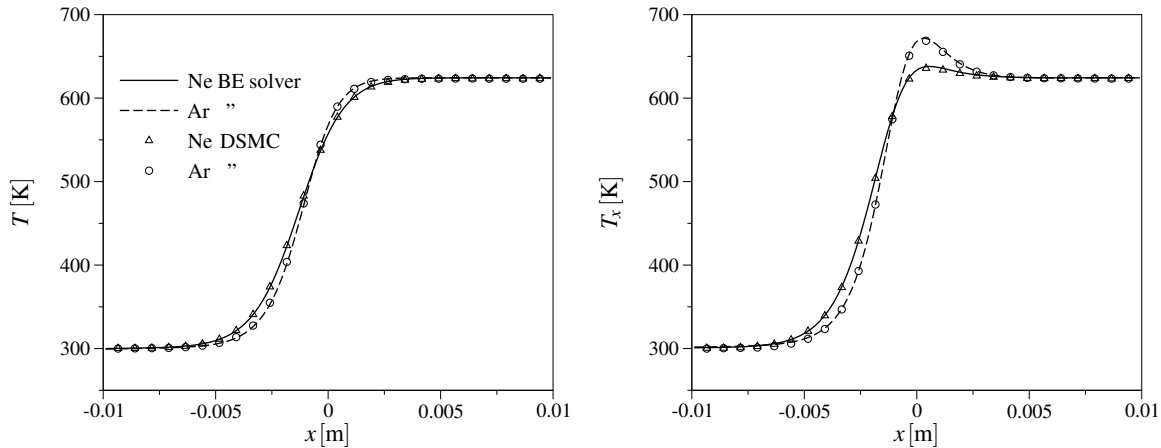


FIGURE 4. Kinetic (left) and parallel (right) temperatures of Ne and Ar (lines BE solver - symbols DSMC).

CONCLUSIONS

An existing spectral-Lagrangian method for the Boltzmann equation has been extended to a multi energy level gas. Preliminary results have been obtained for mixtures of monatomic gases without internal energy. The former have been compared with DSMC results showing excellent agreement. Future work will focus on obtaining results for internal energy excitation (already accounted for in the formulation) and comparison with experimental measurements.

Research of A. M. and T. E. M. is sponsored by the European Research Council Starting Grant #259354, research of J. R. H. is sponsored by the NSF Grant #DMS – 0636586 and research of I. M. G. is sponsored by the NSF Grants #DMS – 1109625 and #DMS – 1107465. The authors would like to thank Mr. Erik Torres at von Karman Institute for providing the DSMC results shown in the paper.

REFERENCES

1. J. H. Ferziger, and H. G. Kaper, *Mathematical theory of transport processes in gases*, North-Holland Pub. Co., 1972.
2. G. A. Bird, *Molecular gas dynamics and the direct simulation of gas flows*, Clarendon, 1994.
3. M. K. Ivanov, A. Kashakovskiy, S. Gimelshein, G. Markelov, A. Alexeenko, Y. Bondar, G. Zhukova, S. Nikiforov, and P. Vashenkov, "SMILE system for 2D/3D DSMC computations," in *Proc. of the 25th Int. Symposium on Rarefied Gas Dynamics*, AIP, 2006.
4. F. G. Tcheremissine, *Comput. Math. Math. Phys.* **46**, 329–343 (2006).
5. P. B. Clarke, P. L. Varghese, and D. B. Goldstein, "A novel discrete velocity method for solving the Boltzmann equation including internal energy and variable grids in velocity space," in *Proc. of the 28th Int. Symposium on Rarefied Gas Dynamics*, AIP, 2012.
6. I. M. Gamba, and S. H. Tharkabhushanam, *J. Comput. Math.* **28**, 430–460 (2010).
7. F. Filbet, and G. Russo, *J. Comput. Phys.* **186**, 457–480 (2003).
8. V. I. Kobolov, R. R. Arlsanbekov, V. V. Aristov, A. A. Frolova, and S. A. Zabelok, *J. Comput. Phys.* **223**, 589–608 (2007).
9. T. E. Magin, M. Massot, and B. Graille, "Hydrodynamic model for molecular gases in thermal non-equilibrium," in *Proc. of the 28th Int. Symposium on Rarefied Gas Dynamics*, AIP, 2012.
10. A. V. Bobylev, *Dokl. Akad. Nauk SSSR* **225**, 1041–1044 (1975), in Russian.
11. J. R. Haack, and I. M. Gamba, "High-performance computing for conservative spectral Boltzmann solvers," in *Proc. of the 28th Int. Symposium on Rarefied Gas Dynamics*, AIP, 2012.
12. J. R. Haack, and I. M. Gamba, "Conservative deterministic spectral Boltzmann-Poisson solver near the Landau limit," in *Proc. of the 28th Int. Symposium on Rarefied Gas Dynamics*, AIP, 2012.
13. C. Hirsch, *Numerical computation of internal and external flows*, Wiley, 1988.
14. B. van Leer, *J. Comput. Phys.* **32**, 101–136 (1979).
15. V. Giovangigli, *Multicomponent flow modeling*, Birkhäuser, 1999.
16. B. Chapman, G. Jost, and R. van der Pas, *Using OpenMP*, MIT press, 2008.
17. GSL - GNU Scientific Library, <http://www.gnu.org/software/gsl/> (2012), [Online; accessed 07-August-2012].
18. M. Frigo, and S. G. Johnson, *Proc. of the IEEE* **93**, 216–231 (2005).
19. E. Torres, and T. E. Magin, "Statistical simulation of internal energy exchange in shock waves using explicit transition probabilities," in *Proc. of the 28th Int. Symposium on Rarefied Gas Dynamics*, AIP, 2012.